

available at www.sciencedirect.comjournal homepage: www.elsevier.com/locate/jmbbm

Research paper

Mechanical properties and the laminate structure of *Arapaima gigas* scales

Y.S. Lin^{a,b}, C.T. Wei^a, E.A. Olevsky^b, Marc A. Meyers^{a,*}^a University of California, San Diego, La Jolla, 92093-0411 CA, United States^b San Diego State University, San Diego, CA, United States

ARTICLE INFO

Article history:

Received 22 September 2010

Received in revised form

6 March 2011

Accepted 18 March 2011

Published online 31 March 2011

Keywords:

Arapaimas

Scale

Collagen

Hydroxyapatite

ABSTRACT

The *Arapaima gigas* scales play an important role in protecting this large Amazon basin fish against predators such as the piranha. They have a laminate composite structure composed of an external mineralized layer and internal lamellae with thickness of 50–60 μm each and composed of collagen fibers with $\sim 1 \mu\text{m}$ diameter. The alignment of collagen fibers is consistent in each individual layer but varies from layer to layer, forming a non-orthogonal plywood structure, known as Bouligand stacking. X-ray diffraction revealed that the external surface of the scale contains calcium-deficient hydroxyapatite. EDS results confirm that the percentage of calcium is higher in the external layer. The micro-indentation hardness of the external layer (550 MPa) is considerably higher than that of the internal layer (200 MPa), consistent with its higher degree of mineralization. Tensile testing of the scales carried out in the dry and wet conditions shows that the strength and stiffness are hydration dependent. As is the case of most biological materials, the elastic modulus of the scale is strain-rate dependent. The strain-rate dependence of the elastic modulus, as expressed by the Ramberg–Osgood equation, is equal to 0.26, approximately ten times higher than that of bone. This is attributed to the higher fraction of collagen in the scales and to the high degree of hydration (30% H_2O). Deproteinization of the scale reveals the structure of the mineral component consisting of an interconnected network of platelets with a thickness of $\sim 50 \text{ nm}$ and diameter of $\sim 500 \text{ nm}$.

© 2011 Elsevier Ltd. All rights reserved.

1. Introduction

Arapaima gigas is one of the largest freshwater fish in the world, reaching a length of about 2–2.5 m and a mass over 150 kg. The fish inhabits the Amazon River Basin in South America. Interestingly, it lives in harmony with the piranha, fish known for their voraciousness and sharp teeth. It has been proposed that the scales of Arapaimas serve

as an armor-like protection against the sharp piranha teeth (Currey, 2010). This function of scales as armor has been demonstrated for *Polypterus senegalus* (Song et al., in press).

A number of studies on fish scales have been conducted addressing the structural arrangement, and collagen formation and orientation (Zylberberg and Nicolas, 1982; Zylberberg et al., 1988, 1992; Olson and Watabe, 1980). Most fish scales have similar material components to other hard tissues such

* Corresponding author. Tel.: +1 858 534 4719; fax: +1 858 534 5698.
E-mail address: mameyers@ucsd.edu (M.A. Meyers).

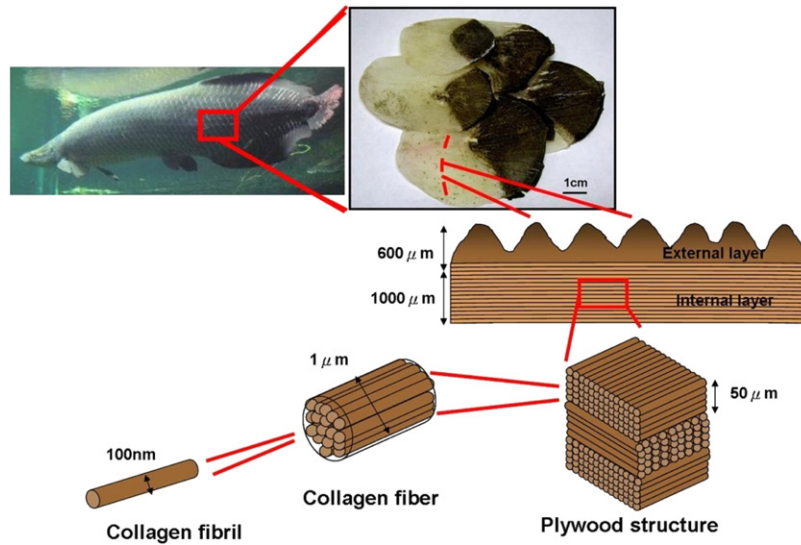


Fig. 1 – Hierarchical structure of the *Arapaima gigas* scales. The *Arapaima gigas* scales have an outside layer that is highly mineralized; the inside is a laminate composite of collagen fibers, which are, on their turn, formed by fibrils.

as bones and teeth. They are mainly composed of type I collagen fibers and calcium-deficient hydroxyapatite, which are also found in bones and teeth. The collagen fibers are usually densely packed lamellae with different orientations from layer to layer, forming a plywood structure (Zylberberg et al., 1992; Weiner and Wagner, 1998). As is also the case for the *Pagrus major* scales reported by Ikoma et al. (2003).

The dimensions of the laminates vary with the thickness of the scale. In *P. reticulata* (guppy), the lamellae are $\sim 1 \mu\text{m}$ thick; in *C. auratus* (goldfish), they are around $5 \mu\text{m}$ (Bigi et al., 2001). Both orthogonal and double twisted plywood patterns are reported. The angles between layers have also been found to vary from 36° for teleosts, to 90° for *Poecilia reticulata* and *Pagrus major* (Zylberberg et al., 1988), to less than 90° for *H. bimaculatus*. This plywood structure has been proposed to form a Bouligand arrangement, named after Bouligand (1972) who studied it extensively. It consists of the superposition of layers with the fibers forming a helical pattern. This structure can also form in the cylindrical geometry (e.g., bones) and in this case each layer is composed of fibers that twist around the axis with a different 'pitch'. Neville (1993) dedicates a considerable portion of his book to these helical and helicoidal arrangements of fibers, which are prevalent in arthropods, fish scales, bone, and wood. He discusses different stacking sequences in fish scales.

The mechanical properties of some fish scales have been studied. Nano-indentation results on *Polypterus senegalus* scales were reported by Bruet et al. (2008) showing that distinct reinforcing layers with different moduli and hardness offer a unique protection mechanism. The external surface layer of this dermal armor consists of ganoin, with a nano-indentation hardness superior to that of enamel: 4.4 GPa. The tensile strength of the scale of *Pagrus major* was measured and found to be $\sim 90 \text{ MPa}$; the elastic modulus was 2.2 GPa. There is also one study on the *Arapaima* scales (Torres et al., 2008), which has only limited tensile data.

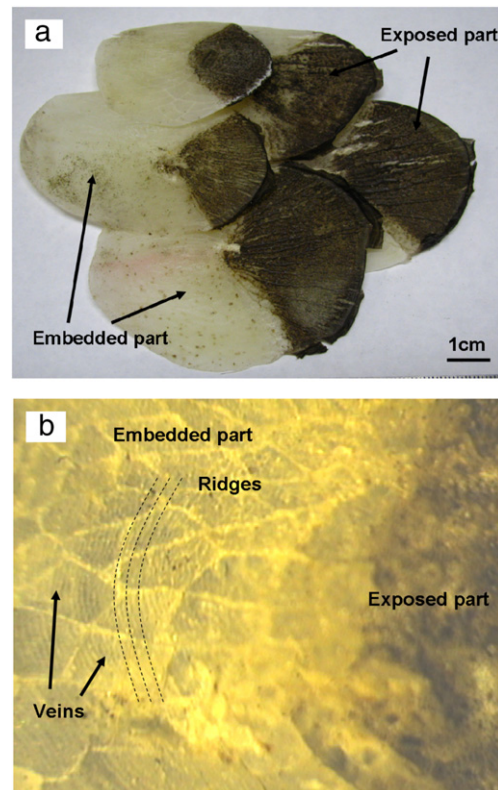


Fig. 2 – (a) Five superposed *Arapaima gigas* scales; embedded (left, light) and exposed (right, dark) and regions are clearly seen, the light regions being larger than the darker ones; (b) Optical micrograph of part of scales showing pattern of veins and circular ridges (embedded part on the left). The ridges are accentuated by dashed lines and are barely visible. The veins form an irregular pattern. They are seen in greater detail in Fig. 3.

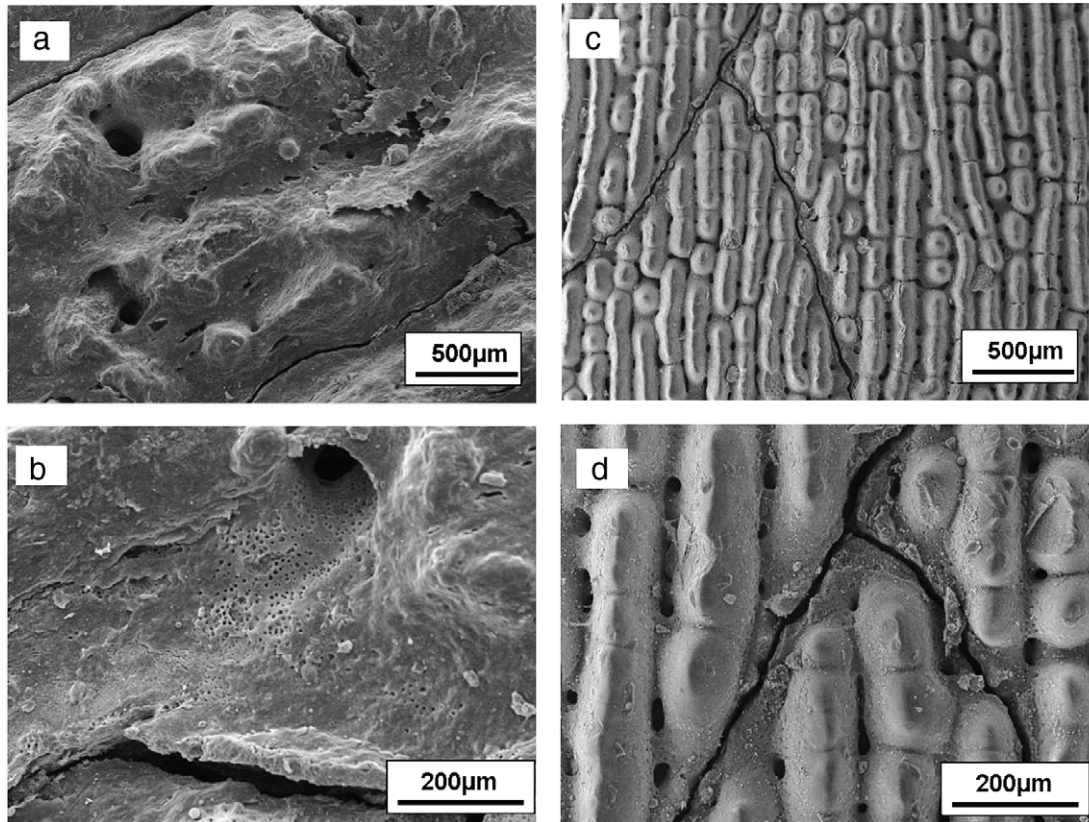


Fig. 3 – SEM images of the mineralized external surface showing the ridge structure on the surface. (a), (b) exposed region of the scale under low and high magnifications; ridges approximately 1 mm wide (c), (d) embedded part of the scale; ridges ~0.2 mm wide.

Both the hydration and strain rate play a significant role in the mechanical properties of biological materials. Therefore, tensile tests were conducted in wet and dry conditions and at different strain rates to investigate how they affect the mechanical properties of the scales. Thus, the objective of this study was to establish the effects of strain rate and hydration on the scales.

2. Experimental procedure

Mechanical tests including tensile and micro- and nano-indentation were conducted. Scanning electron microscopy was performed on the fracture surfaces of tensile test specimens, cross sections and surfaces of the scales to establish its structure. Both EDX and XRD were used to identify the chemical content and scale composition.

2.1. Tensile tests

The air-dried scales were extracted from the lateral part of the *Arapaima gigas* and rehydrated by placing them in distilled water for four days before tensile testing. Specimens were cut from the embedded part of the scale into dog-bone shape by a programmed laser cutting machine to fit into the custom-made grips. Their dimensions were 25.4 mm

in length, 6.35 mm in width, 6.35 mm in gage length and 2.29 mm in gage width. The specially designed fixture was composed of two grips and a sliding track. Both the upper and lower grips were confined in the track to minimize torsion and misalignment. The fixture is described by Lin and Meyers (2009). Testing was conducted in an Instron 3346 single column testing system equipped with a 500 N load cell. The hydrated samples were tested immediately after they were immersed in water for 4 days. The strain rate used for hydrated samples was varied from 10^{-4}s^{-1} to 10^{-2}s^{-1} .

2.2. Micro- and nano-indentation tests

Cross-sectional specimens were cut from the exposed region of the *Arapaima gigas* scale with a thickness of about 2 mm. Both the specimens for micro- and nano-indentation were in air-dried condition with water content of ~16 wt%. The samples were mounted in epoxy, ground to expose the cross-section surface with sand paper, and polished to $0.5\ \mu\text{m}$ with an Al_2O_3 solution. An LECO M-400-H1 hardness testing machine equipped with a Vickers indenter was used. A load of 25 N was utilized to indent the cross section starting from the internal layers to the external layer. Nine linear indentations were made in three different areas with a total of 27 indentations. The interval distance between indentations was sufficiently large to prevent the residual stress and strain hardening effect.

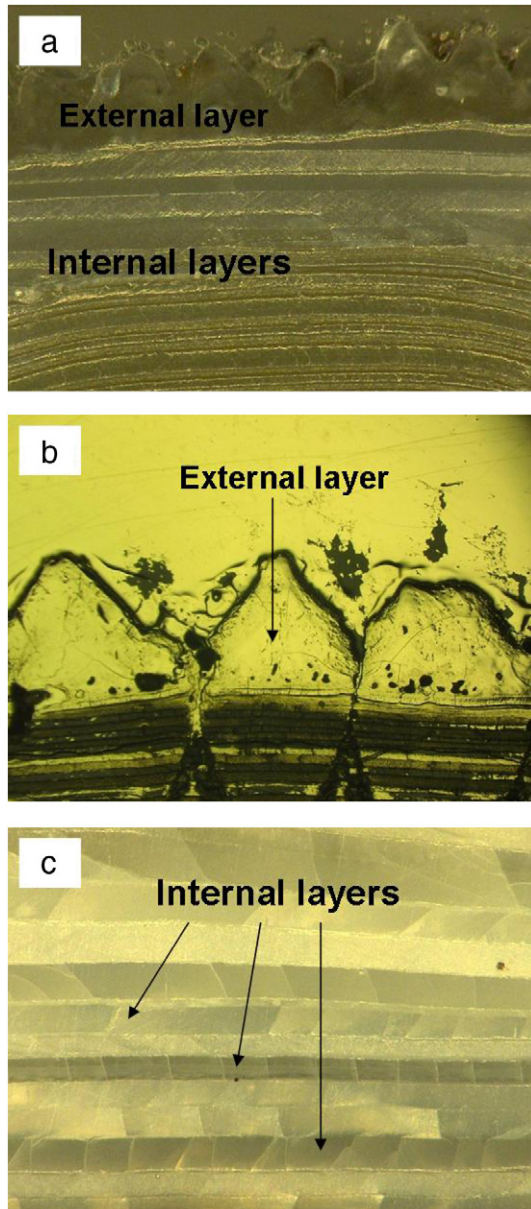


Fig. 4 – Optical micrographs of cross section of scale:
(a) Overview of the entire scale at a lower magnification
(b) Higher magnification of external layer showing ridge geometry;
(c) Higher magnification of internal layers showing laminate structure in the scale.

Nano-indentation was also conducted on the cross section of the scale. A Berkovich tip was employed on the polished flat cross section of the scale to measure the indent resistance including the elastic modulus and hardness through the different layers which comprise the individual scale. The applied maximum force was 500 μN with loading rate of 50 $\mu\text{N}/\text{min}$.

2.3. Microstructure characterization

Both the fracture and polished cross-section surface of the scale were characterized by using a field emission scanning

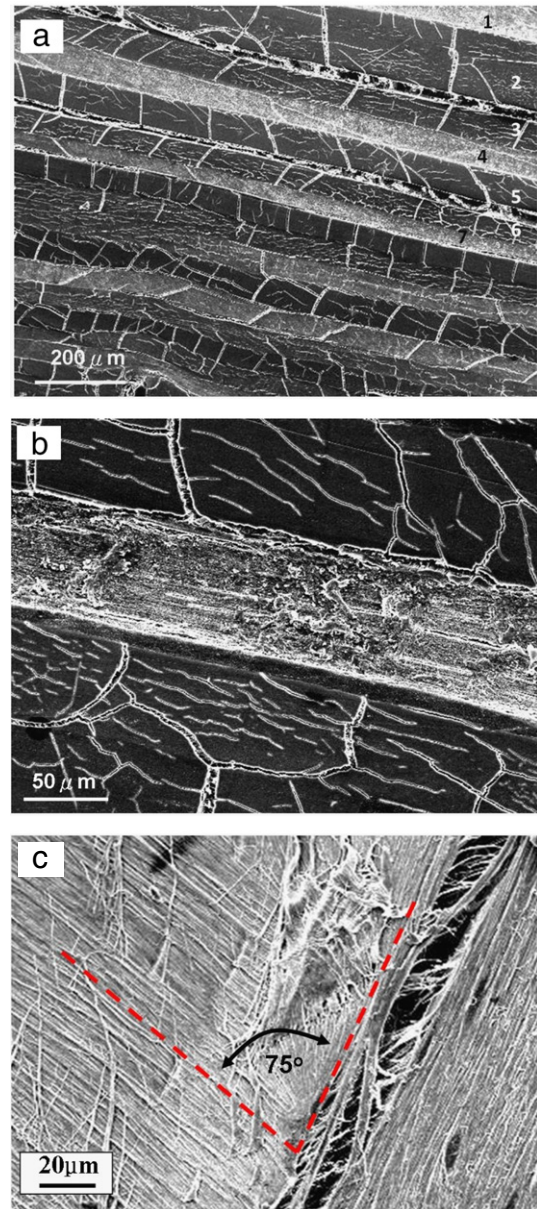


Fig. 5 – (a) SEM image of the cross section showing the laminated structure in the internal layers. The white lines in the SEM image represent the cracks due to the drying of the scale. It can be seen that, as we go from the top to bottom, that Layers 1, 4, and 7 do not show cracks;
(b) Higher magnification SEM image of cross section showing the collagen fibril orientation. The aligned collagen fibers can be seen in the middle lamella; no cracks were formed perpendicular to fiber axis;
(c) top view showing two adjacent layers and angle between them.

electron microscope (FEI-XL30, FEI Company, Oregon, USA) equipped with electron-dispersive X-ray spectroscopy (EDS). The samples were gold coated and observed with secondary electron mode at a 10 kV accelerating voltage. Elemental analysis was conducted on the cross section of the scale by EDS to verify the element content and differentiate between the internal and external layers.

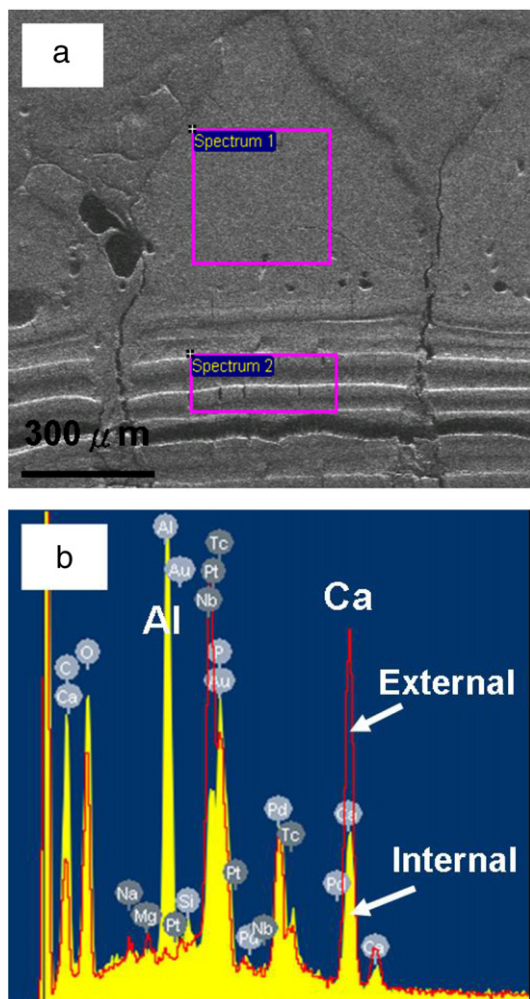


Fig. 6 – (a) Back scattered image of the polished cross section of scale; cracks are produced by drying; (b) EDS results of external and internal regions of the cross section; notice that calcium peak is more pronounced for external layer.

2.4. X-ray diffraction

X-ray diffraction (MiniFlex™ II, Rigaku Company, Texas, USA) with the Cu $K\alpha_1$ radiation source was performed on the two sides of *Arapaima* scales. In order to obtain better diffraction conditions, both the outer and inner surfaces were polished. The wavelength of the radiation source is 0.154 nm. The scan angle ranged from 20° to 60° with step sizes of 0.01° at a rate of 1°/min.

2.5. Fourier transform infrared spectroscopy

Fourier transform infrared spectroscopy (FTIR) was used to analyze the chemical compounds in the scale with different absorption peaks which correspond to different frequencies of vibration of bonds between the atoms. The sample, with dimensions of 1 × 1 cm, was cut from the embedded part of the scale and ground to a thickness of 300 μm. A Varian Excalibur 3100 FTIR spectrometer with wave number of

20 cm⁻¹ spectral resolution was used to identify the chemical compounds in the scale. The sample was tested in Attenuated Total Reflectance (ATR) mode with ATR configuration of Si and ZnSe plate equipped in the FTIR instrument.

2.6. Characterization of deproteinized *Arapaima gigas* scales

Both mineral and collagen are the key extracellular components of the scale. In order to investigate the structure of the mineral phase in the scale, the specimens were immersed in a 2.6 wt% NaOCl solution (Weiner and Price, 1986) for 7 days to remove the protein in the scale.

3. Results and discussion

The *Arapaima* scale has two main distinguishable sections: an embedded part with a thickness of ~1 mm and an exposed section of ~2 mm in thickness. It is thicker than most other fish scales, that can be as low as 1–2 μm in the case of *Pagrus major* (Ikoma et al., 2003). Fig. 1 shows the hierarchical structure of the *Arapaima gigas* scales. The scale has a laminate structure composed of an external layer (highly mineralized) with ridges and internal layers. The main building block of the scales is collagen fibers forming a plywood structure. The collagen fibrils, with a diameter of ~100 nm, form collagen fibers with a diameter of 1 μm. The collagen fibers, in turn, assemble into lamellae with a thickness of ~50 μm.

3.1. Structure characterization

Fig. 2 shows the typical arrangement of the fish scales. The scales, with dimensions of 5–7 cm in length (and, in large fish, up to 10 cm) and ~4 cm in width, overlap one another to form the characteristic armor-like protection. The darker region is exposed to water, while the lighter areas are the embedded regions which are covered by other scales. The areal fraction of the lighter (covered) regions is approximately ~0.6, consistent with the fact that, in average, there are three layers overlapping each other. Note that these regions are mislabeled in Figure 5 of Torres et al. (2008). The ridge structure is oriented along the partial circle contour around the focus point on the junction of exposed and embedded parts. Fig. 2(b) is an optical micrograph showing the veined pattern in the embedded part of the scale. There are also circular lines drawn, marking the presence of ridges. *Arapaima* scales are commonly used as nail files in the Amazon basin and these ridges act as controlled grooves. They are perpendicular to the longitudinal axis of the scales. Fig. 3(a) and (b) are SEM images of the exposed part of surface and Fig. 3(c) and (d) are SEM images of the embedded part. Fig. 3(c) and (d) show the ridge structure which corresponds to circles drawn in Fig. 2(b). The spacing between the ridges in the exposed part is larger than that in the covered part of the scale. The scale thickness is correspondingly larger for the exposed part.

By optical microscopy of the cross section, one can observe the external and internal layers (Fig. 4). The corrugated

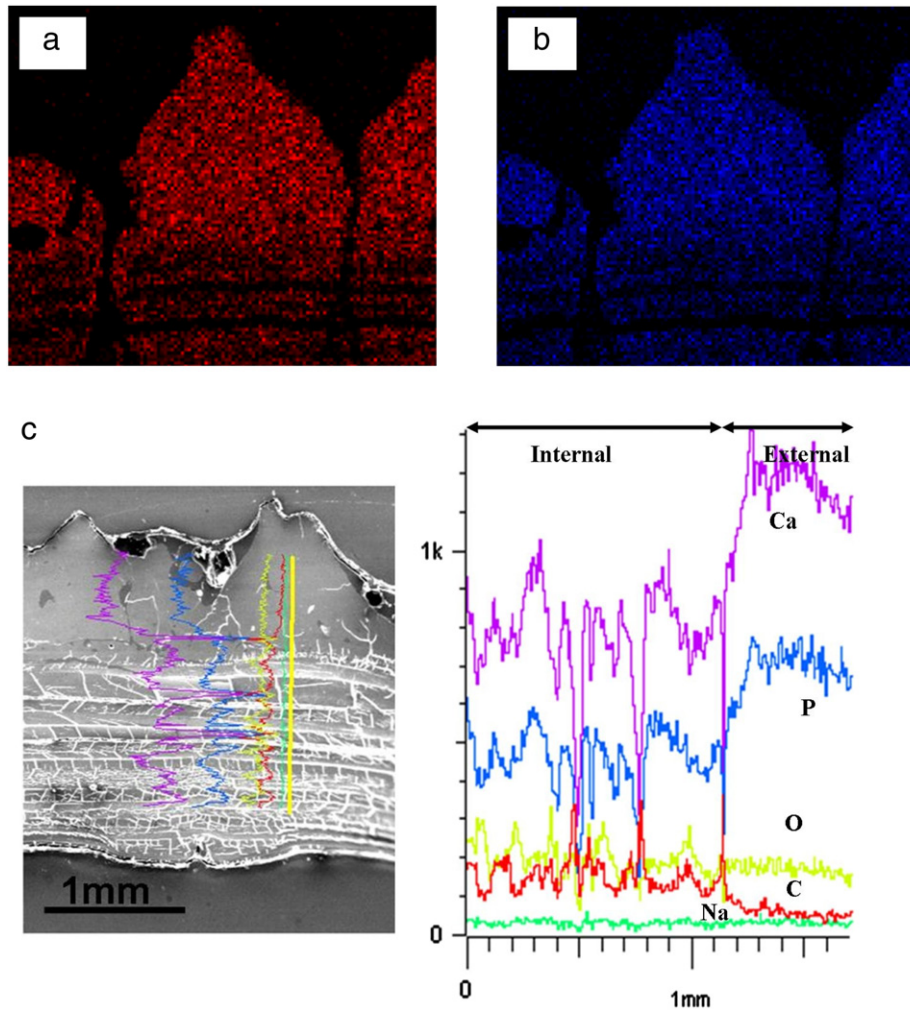


Fig. 7 – (a) Calcium mapping of the cross section of the scale; (b) Phosphorous mapping of the cross section of the scale; (c) Line scans of calcium and phosphorous along cross section. It can be seen that both calcium and phosphorous concentrations are higher in the external layer.

surface of external layer corresponds to the ridge structure of the surface, whereas the internal layers are characterized by lamellae.

Macroscopically, the exposed part shows a rougher surface than the embedded part. Nevertheless, the ridge-like structure is distributed across the entire embedded (covered) part. Additionally, it can be observed that the thickness of the scale gradually decreases toward the edge of the embedded region. The average thickness of the exposed part is about 1.8 mm and that of the internal part is ~ 1 mm. Fig. 5(a) shows the internal layers of the scale with the lamellar structure having an approximate layer thickness of $50\ \mu\text{m}$. At higher magnification (Fig. 5(b)), the central lamella shows collagen fibrils oriented in one direction. There is a profuse network of cracks in the layers due to the drying process. These cracks propagate between the fibers and are due to shrinking stresses. When the fibers are oriented parallel to the surface, no cracks can be seen. In Fig. 5(a) the layers are numbered. Layers 1, 4, and 7 do not exhibit cracks. Thus, this suggests an angle between layers of approximately $60^\circ (3 \times 60^\circ = 180^\circ)$. Fig. 5(c) shows a top view of the scale; one can see the

layers. The angle between them is $\sim 75^\circ$; consistent with the periodicity in the crack pattern seen in Fig. 5(a).

Fig. 6(a) is the BSE image of the polished cross section. Energy-dispersive X-ray spectroscopy was conducted on two spots, in the external and internal layers. The EDS results (Fig. 6(b)) show that the calcium content in external region is about twice of that in internal region. The Al peak is due to Al_2O_3 polishing particles. Calcium and phosphorous mapping was also conducted on the cross section and the amount of these elements gradually decrease from the external to the internal layer. (Fig. 7(a) and (b)). This higher mineralization is responsible for a higher hardness value in the external region. Fig. 7(c) shows calcium and phosphorous line scans. It is evident that the surface is richer in these elements.

Fig. 8(a) shows the structure of the scales after deproteinization. The mineral phase of the scale shows a platelet morphology. The mineral platelets have a random orientation and are the characteristic elements of the entire deproteinized scale structure. Each plate has dimensions of $50\ \text{nm}$ thickness and $500\ \text{nm}$ diameter. These plates form assemblies that are connected. Fig. 8(b) shows the most common

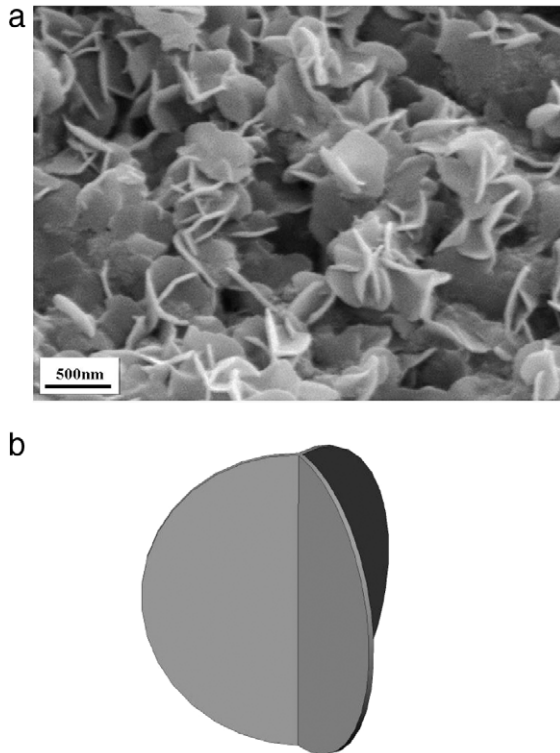


Fig. 8 – SEM micrographs of the deproteinized scale: (a) Mineral disks with approximate diameter of 500 nm and thickness of 50 nm; (b) Schematic drawing showing disk with three lobes.

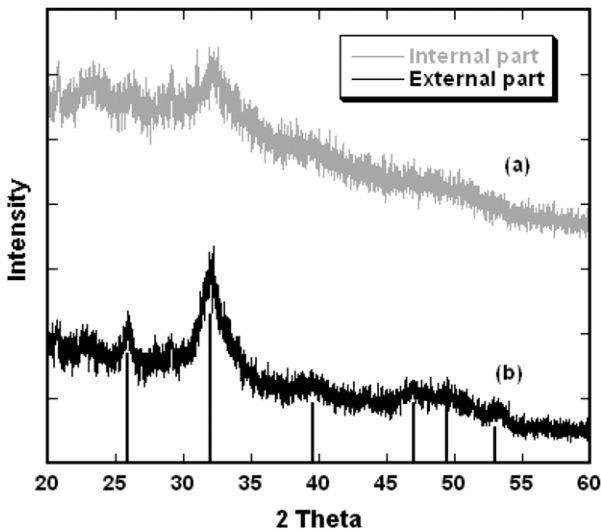


Fig. 9 – X-ray diffraction patterns from scale: (a) internal part; (b) external part with strong hydroxyapatite peaks. The XRD pattern can be indexed to standard hydroxyapatite (JCPDS#00-001-1008, 0000).

configuration of the platelets, which we assume to be three semi-circles connected along a common axis, which we shall name ‘tri-disk’. This arrangement is well suited for the min-

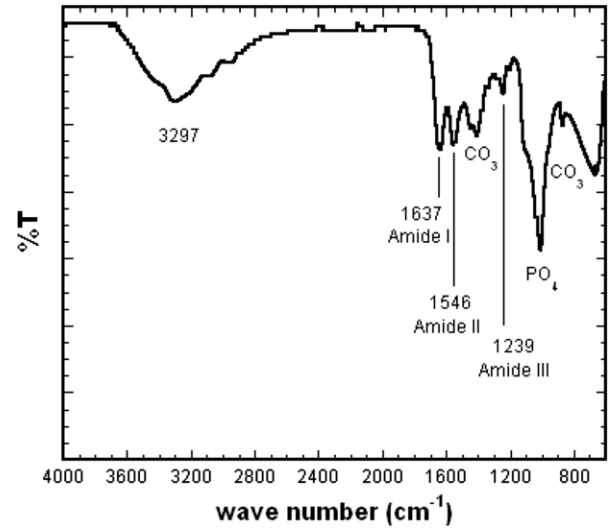


Fig. 10 – FTIR spectra of *Arapaima gigas* scale showing amide I, II, and III of type I collagen, phosphate groups and carbonate anions.

eral to form a semi-continuous or even continuous network in the aligned collagen fiber network. It can be envisaged that the axis of the ‘tri-disk’ in Fig. 8(b) would be aligned with the collagen fibrils. Thus, the presence of the mineral does not disturb the parallel arrangement of the collagen. It is possible to estimate the density of these platelets that is required to form a continuous network by assuming contiguous spheres into which the trifles are inscribed. This is less than 0.1.

XRD was conducted on the polished internal and external surfaces of the fish scales. Fig. 9 shows the two XRD patterns with 2θ scan from 20° to 60° . The broad peaks of the XRD pattern indicate that the scale has low crystallinity. The XRD patterns are from (a) the internal surface and (b) the external surface. The peaks in the internal surface are not as obvious as those in the external surface. The peaks at 2θ of 25.9° , 31.9° , 39.8° , 47.2° , 49.3° , and 53.2° correspond to d spacings of 0.343, 0.281, 0.226, 0.193, 0.185, and 0.172 nm, respectively. The XRD results are consistent with the results by Torres et al. (2008) which are 25.8° , 31.8° , 39.6° , 47.2° , 49.3° , and 53.1° corresponding to d spacings of 0.345, 0.281, 0.227, 0.192, 0.184, and 0.172 nm. The XRD results of the scales can also correspond to the hydroxyapatite XRD, which has peaks at $2\theta = 25.8^\circ$, 31.8° , 39.6° , 47.2° , 49.3° , and 53.1° . The peaks are also consistent with results from Ikoma et al. (2003).

FTIR spectroscopy shows several strong absorption peaks, similar to previous studies (Ikoma et al., 2003; Torres et al., 2008). The absorption peaks at 1637 , 1546 , and 1239 cm^{-1} are the three characteristic peaks which correspond to amide I, amide II, and amide III of type I collagen (Thomas et al., 2007; Pati et al., 2010) (Table 1). Peaks at around 1000 cm^{-1} , which represent the phosphate groups at 872 , 1401 , and 1450 cm^{-1} and correspond to carbonate anions, were also observed. Thus, the scale is composed of organic (type I collagen) and inorganic components (calcium-deficient hydroxyapatite) (Fig. 10).

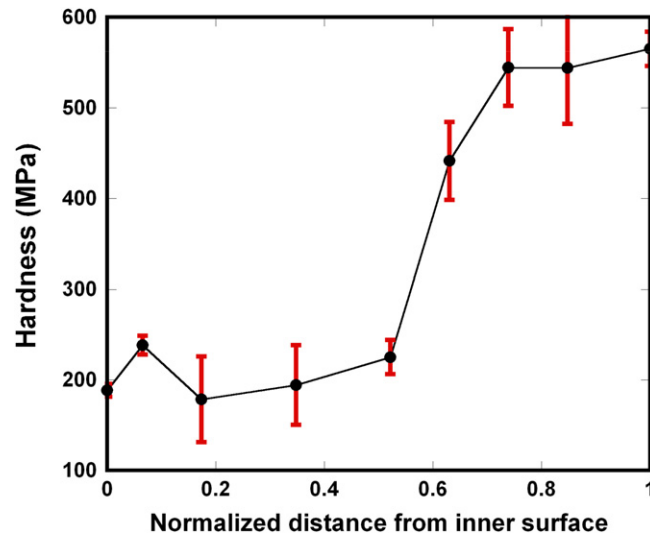


Fig. 11 – Micro-indentation hardness through the cross section of scale; measurements start at inner surface and proceed to outer surface. Hardness is significantly higher in the external layer.

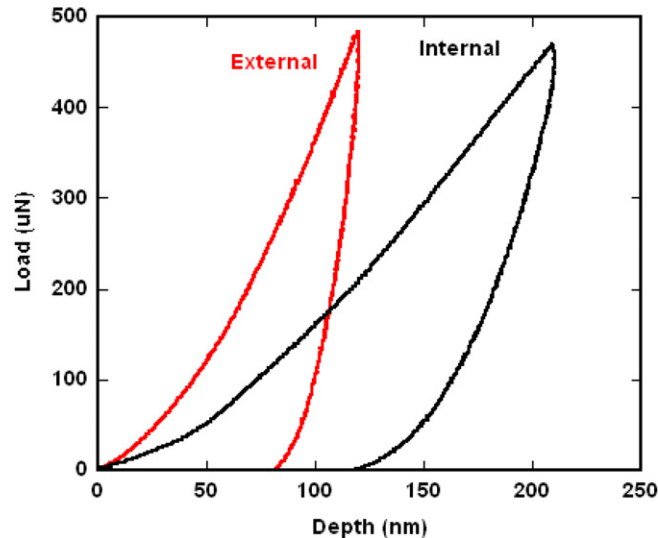


Fig. 12 – Typical nano-indentation curves for external and internal layers. Notice higher slope for external layer, indicative of higher Young's modulus, and larger hysteresis in inside layer, indicative of greater deformation and lower hardness.

Table 1 – Comparison of wavenumbers of amide I, II and III.

	Torres et al., 2008	Ikoma et al., 2003	Present study
Amide I (cm^{-1})	1662	1657	1637
Amide II (cm^{-1})	1560	1520	1546
Amide III (cm^{-1})	1242	1447	1239

3.2. Micro- and nano-indentation testing

The average hardness value in the internal layers was found to be 200 MPa, increasing to about 550 MPa in the external layer. Fig. 11 shows the micro-indentation hardness through the cross section of the exposed region of the scale. The hardness of the external layer is over twice that of the internal

layer. This large difference suggests that the purpose of the external layer is to serve as protective armor against the sharp teeth of the piranha. Bruet et al. (2008) found that the scales from *Polypterus senegalus* also exhibit a multiple layer structure. They performed nano-indentation testing on the scales and showed that the hardness increases with distance from the inner surface to the outer surface, from 0.54 GPa to 4.5 GPa.

In order to compare the present results with those of Bruet et al. (2008), nano-indentation tests were performed. Fig. 12 shows the load–depth curves. The internal region of the scale exhibits lower hardness (0.6 GPa) than the external region (2 GPa). This is the direct result of the high mineral content in the external layer. Whereas the internal region has a value comparable with that of Bruet et al. (2008), the external region is much softer, the reason being that the

Table 2 – Nano-indentation values.

	External	Internal
Nano-hardness (GPa)	2.0 ± 0.4	0.6 ± 0.08
Elastic modulus (GPa)	46.8 ± 8.9	16.7 ± 4.0

Table 3 – Tensile test values.

	Ultimate tensile strength (MPa)	Elastic modulus (GPa)
Dry scale	46.7 ± 4.6	1.2 ± 0.2
Hydrated scale	25.2 ± 7.3	0.1 ± 0.02

external layer in *Polypterus* is the biomineral ganoin. Table 2 summarizes the average results of nano-hardness and elastic modulus of internal and external layers.

3.3. Tensile properties

Fig. 13 shows the typical tensile stress–strain curves in (a) dry and (b) hydrated conditions. The differences are striking. The stress–strain curve for dry condition shows a much steeper slope than that of hydrated condition demonstrating a higher elastic modulus. The elastic modulus for the dry condition is about 1.2 GPa, whereas for the hydrated condition it is one tenth of this, about 0.1 GPa. The dry samples also demonstrate higher ultimate tensile strength, about 46.7 MPa, while that in the hydrated samples is 25.2 MPa. Conversely, the hydrated scales show a much higher deformation to failure. The maximum tensile strain of the dehydrated condition is less than 10%. In contrast, the maximum tensile strain of the hydrated condition is 30%–40%. The flexibility of the scales is clearly needed during swimming, so that they can flex with the body of the fish (Table 3).

The tensile strengths obtained here in both dry and hydrated conditions are in agreement with the test results of Torres et al. (2008) which yielded values of 54 and 22 MPa, respectively. Their curves also exhibited load drops, evidence, as in our experiments, of “graceful” failure. Fig. 13(b) shows, by means of arrows, regions with small load drops, which are attributed to partial failure of the laminates, while the specimens retain their integrity. They can also be due to sliding or separation between layers. To obtain the degree of hydration, samples were weighed and put into the furnace to dehydrate at 105 °C for 2 days. The air-dried sample contained a water concentration of 16% while that of hydrated sample was 30%. In the hydrated condition, the curves are less linear than those in the dry condition.

Ikoma et al. (2003) reported that the tensile strength of *Pagrus major* scales is 93 MPa which is higher than our results. The strength of the *Arapaima gigas* scale in the dry condition is about one half of that of the *Pagrus major*. It is inferred from the low ductility (~5%) that the *Pagrus major* scales were tested in the dry condition. The tensile curve also exhibited a pseudo-plastic behavior, i.e., the curve shows non-linearity prior to failure.

Fig. 14(a) shows the strain-rate sensitivity of the elastic modulus of the scale; it increases from 118 MPa at 10⁻⁴s⁻¹ to 404 MPa at 10⁻²s⁻¹. In Fig. 14(b) these values are plotted to

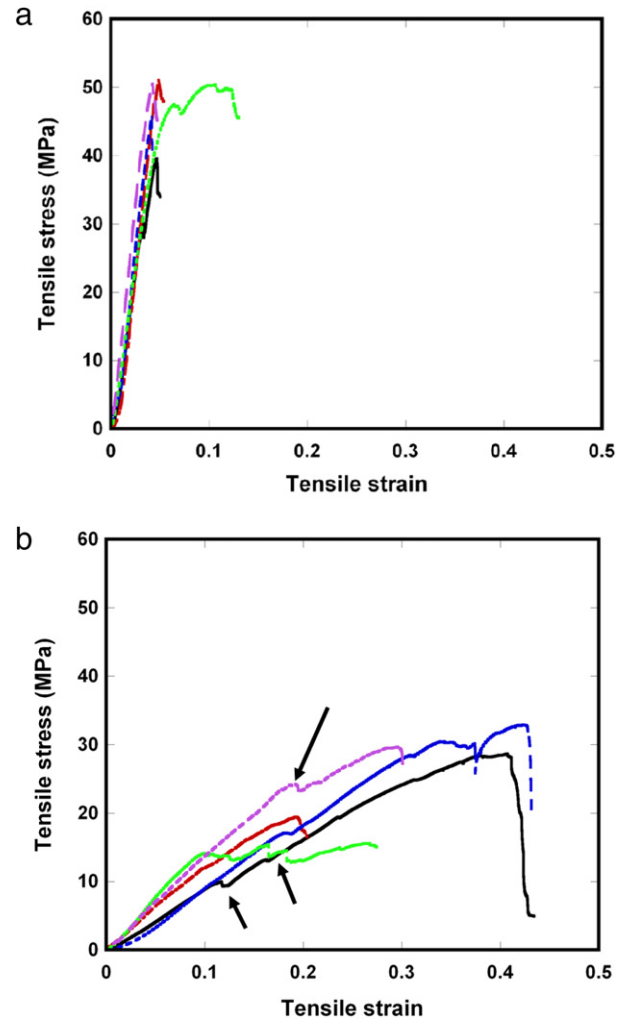


Fig. 13 – Stress–strain curves in tension of specimens aligned with longitudinal axes of scales at a strain rate of 10⁻⁴s⁻¹ in (a) dry and (b) hydrated conditions. Load drops in (b) marked by arrows designate partial failure of laminate structure.

the Ramberg–Osgood equation, which is commonly used to describe the strain-rate sensitivity *d*, of the elastic modulus *E* (e.g., Hight and Brandeau (1983); Wright and Hayes (1976)):

$$E = C(\dot{\epsilon})^d$$

where $\dot{\epsilon}$ is the strain rate and *C* is an experimental parameter. In our results, *C* and *d* are 1.5 GPa and 0.26, respectively. For comparison purposes, the elastic moduli of bone, rat-tail collagen, and horn (keratin) are also plotted. Adharapurapu et al. (2006) obtained values of *C* and *d* of 12 GPa and 0.018, respectively. Horn keratin exhibits a value of *d* equal to 0.19 in transverse direction and 0.12 in longitudinal direction. Thus the parameter *d*, which describes the strain-rate sensitivity in fish scale, is an order higher than that in bovine bone and considerably higher than human femur bone, keratin and rat-tail collagen (McElhaney, 1966; McKittrick et al., 2010; Haut and Little, 1972). The strain-rate sensitivity in most of the biological materials is primarily due to collagen. The high

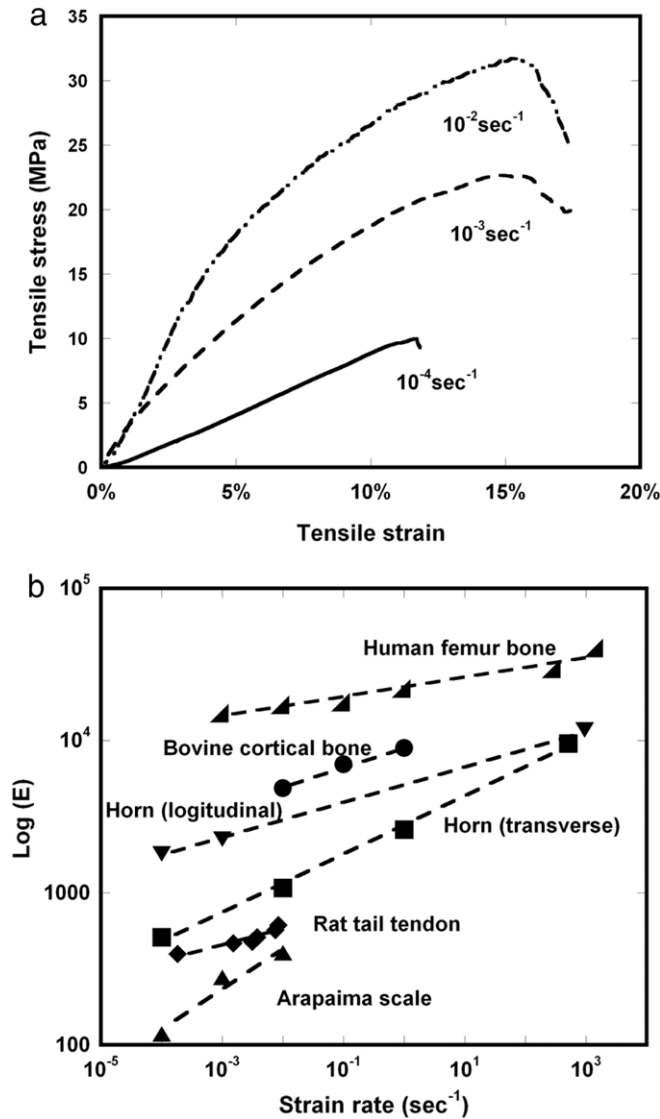


Fig. 14 – (a) Stress–strain curves of hydrated scale at three different strain rates; (b) Elastic modulus as a function of strain rate for a number of biological materials; *Arapaimas* scales have, by virtue of their higher collagen content, the highest strain rate sensitivity of E (Human femur bone: McElhane, 1966; Bovine cortical bone: Adharapurapu et al., 2006; Horn keratin: McKittrick et al., 2010; Rat-tail tendon: Haut and Little, 1972).

strain-rate dependence in the *Arapaima* scales is attributed to the high degree of hydration ($\sim 30\%$) and the much lower mineral content in fish scales (30 wt%) compared with that in bone (65 wt%) (Olszta et al., 2007).

The fracture surface (Fig. 15(a)) clearly shows the different collagen fibril orientations in different lamellae. Collagen fibers in each layer are aligned as described by Onozato and Watabe (1979) and Zylberberg et al. (1992), among others. The angle between two adjacent lamellae seem close to 90° , thus forming a plywood structure. However, the twisted plywood structure (e.g., angle of 60°) is a definite possibility as well. Fig. 15(b) shows pulled-out or distorted collagen fibrils damaged during the tensile testing. Tensile fracture not only breaks the collagen fibers but also tears the collagen fibers away from each other. The fracture mechanism seems to be a combination of the collagen fracture and the pulling out of the collagen fibers in a single layer.

4. Conclusions

Arapaima gigas scales are constructed as a laminate composite structure composed of lamellae with collagen fibers in parallel orientation. The presence of amide I, II, and III, characteristic of type I collagen was confirmed. Each layer is formed by collagen fibers with a diameter of $\sim 1 \mu\text{m}$. The fibers in two adjacent layers are not perpendicular to each other, suggesting a twisted plywood structure (Bouligand arrangement), which consists of a stacking of lamellae in which there is a twisting pattern. This arrangement ensures that the structure has in-plane isotropy in mechanical response. In contrast with tendon, where all the collagen fibers are aligned, the Bouligand pattern ensures in-plane isotropy. The lower maximum strength ($\sim 25\text{--}47 \text{ MPa}$), in comparison with tendon ($\sim 100 \text{ MPa}$) shows that only a portion of the fibers resist the stresses in tension. The low

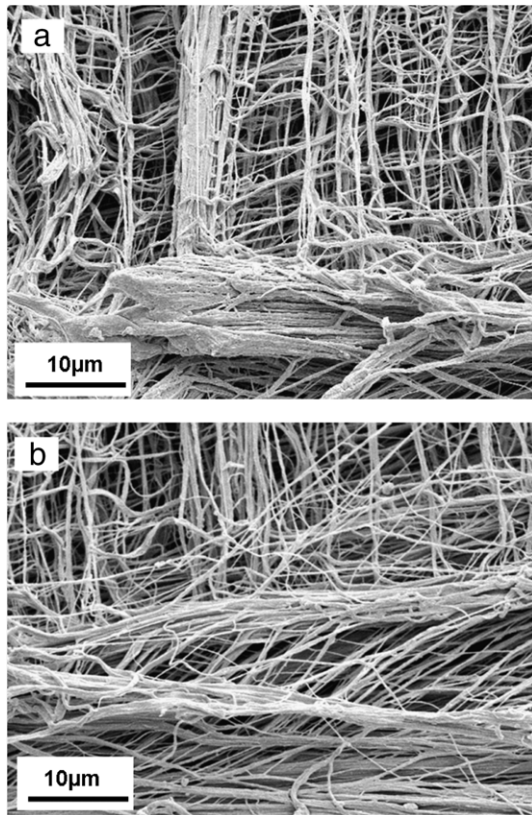


Fig. 15 – (a), (b) SEM image of the fracture surface collagen fibers separated and distorted by the action of tensile forces. The intrachain bonds are covalent, while the interfiber bonds are van der Waals or hydrogen, thereby much weaker.

Young's modulus of the hydrated scales (~ 0.1 GPa) indicates that the collagen fibers must slide past each other in tension. In contrast, Young's modulus of tendon is ~ 1.2 – 1.5 GPa. In line with the Bouligand structure, only a fraction of the collagen fibers are oriented along the tensile axis. If we consider a rotation of approximately 60° – 75° , then one would expect that approximately one third of the fibers are in tension, on average. Thus, the tensile strength should be one third of that of fully aligned, e.g., tendon, consistently with the experimental results. Both the micro- and nano-hardness in the external region are higher than that in the internal region due to the higher mineralization associated with the protection purpose of the scale surface.

Tensile tests in the dry condition show the higher elastic modulus and tensile strength than that in the hydrated condition, which indicates that hydration plays an important role in the mechanical strength of the scale. The elastic modulus of hydrated scales increases significantly as the strain rate increases and can be interpreted by the Ramberg–Osgood equation with an exponent equal to 0.26. The higher strain-rate sensitivity of scales, in comparison with bone, keratin and rat-tail tendon, is proposed to be due to the lower mineral content and the higher degree of hydration of the scales (around 30%). Fracture surface observation reveals that a combination of collagen fiber stretching, sliding and fracturing are the dominant failure mechanisms.

Acknowledgments

We thank Mr. Gaspar Ritter, Kuryala Lodge, Araguaia, for providing us the *Arapaimas* scales and Mr. Marcel de Roure for making all the contacts that made this possible. Without proper specimens this research could not have been conducted. Discussions with Dr. Po-Yu Chen are gratefully acknowledged. The referees contributed significantly through their incisive remarks. This research was funded by NSF DMR Biomaterials Program (Grant DMR 0510138).

REFERENCES

- Adharapurapu, R.R., Jiang, F., Vecchio, K.S., 2006. Dynamic fracture of bovine bone. *Mater. Sci. Eng. C* 26, 1325–1332.
- Bigi, A., Burghammer, M., Falconi, R., Koch, M.H.J., Panzavolta, S., Riekkel, C., 2001. Twisted plywood pattern of collagen fibrils in teleost scales: an X-ray diffraction investigation. *J. Struct. Biol.* 136, 137–143.
- Bouligand, Y., 1972. Twisted fibrous arrangements in biological materials and cholesteric mesophase. *Tissue Cell* 189–217.
- Bruet, B.J.F., Song, J., Boyce, M.C., Ortiz, C., 2008. Materials design principles of ancient fish armour. *Nat. Mater.* 7, 748–756.
- Currey, J.D., 2010. Mechanical properties and adaptations of some less familiar bony tissues. *J. Mech. Behav. Biomed. Mater.* 3, 357–372.
- Haut, R.C., LITTLE, R.W., 1972. A constitutive equation for collagen fibers. *J. Biomech.* 5, 423–430.
- Hight, T.K., Brandeau, J.F., 1983. Mathematical modeling of the stress strain-strain rate behavior of bone using the Ramberg–Osgood equation. *J. Biomech.* 16, 445–450.
- Ikoma, T., Kobayashi, H., Tanaka, J., Wals, D., Mann, S., 2003. Microstructure, mechanical, and biomimetic properties of fish scales from *Pagrus major*. *J. Struct. Biol.* 142, 327–333.
- Joint Committee on Powder Diffraction Standards, Associateship at the National Bureau of Standards. Powder diffraction data: no. 00-001-1008. Swarthmore, PA: JCPDS; 1076.
- Lin, A.Y.M., Meyers, M.A., 2009. Interfacial shear strength in abalone nacre. *J. Mech. Behav. Biomed. Mater.* 2, 607–612.
- McElhaney, J.H., 1966. Dynamic response of bone and muscle tissue. *J. Appl. Physiol.* 21, 1231–1236.
- McKittrick, J., et al., 2010. Energy absorbent natural materials and bioinspired design strategies: a review. *Mater. Sci. Eng. C* 30, 331–342.
- Neville, A.C., 1993. *Biology of Fibrous Composites*. Cambridge University Press, UK.
- Olson, P., Watabe, N., 1980. Studies on formation and resorption of fish scales. *Cell Tissue Res.* 211, 303–316.
- Olszta, M.J., Cheng, X., Jee, S.S., Kumar, R., Kim, Y.Y., Kaufman, M.J., 2007. Bone structure and formation: a new perspective. *Mater. Sci. Eng. R* 58, 77–116.
- Onozato, H., Watabe, N., 1979. Studies on fish scale formation and resorption. *Cell Tissue Res.* 201, 409–422.
- Pati, F., Adhikari, B., Dhara, S., 2010. Isolation and characterization of fish scale collagen of higher thermal stability. *Bioresour. Technol.* 101, 3737–3742.
- Song, J., Ortiz, C., Boyce, M.C., 2011. Threat-protection mechanics of an armored fish. *J. Mech. Behav. Biomed. Mater.*, in press (doi:10.1016/j.jmbbm.2010.11.011).
- Thomas, V., Dean, D.R., Jose, M.V., Mathew, B., Chowdhury, S., Vohra, Y.K., 2007. Nanostructured biocomposite scaffolds based on collagen coelectrospun with nanohydroxyapatite. *Biomacromolecules* 8, 631–637.

- Torres, F.F., Troncoso, O.P., Nakamatsu, J., Grande, C.J., Gomez, C.M., 2008. Characterization of the nanocomposite laminate structure occurring in fish scales from *Arapaima Gigas*. *Mater. Sci. Eng. C* 28, 1276–1283.
- Weiner, S., Wagner, H.D., 1998. The material bone: structure-mechanical function relations. *Annu. Rev. Mater. Sci.* 28, 271–298.
- Weiner, S., Price, P.A., 1986. Disaggregation of bone into crystals. *Calcified Tissue Int.* 39, 365–375.
- Wright, T.W., Hayes, W.C., 1976. Tensile testing of bone over a wide range of strain rates: effects of strain rate, microstructure and density. *Med. Biol. Eng. Comput.* 14, 671–679.
- Zylberberg, L., Bereiter-Hahn, J., Sire, J.Y., 1988. Cytoskeletal organization and collagen orientation in the fish scales. *Cell Tissue Res.* 253, 597–607.
- Zylberberg, L., Bonaventure, J., Cohen-Solal, L., Hartmann, D.J., Bereiter-Hahn, J., 1992. Organization and characterization of fibrillar collagens in fish scales in situ and in vitro. *J. Cell Sci.* 103, 273–285.
- Zylberberg, L., Nicolas, G., 1982. Ultrastructure of scales in a teleost (*Carassius auratus* L.) after use of rapid freeze-fixation and freeze-substitution. *Cell Tissue Res.* 223, 349–367.